Brain, Behavior, and Immunity 134 (2026) 106297

Contents lists available at ScienceDirect

Brain Behavior and Immunity

journal homepage: www.elsevier.com/locate/ybrbi

Insights into mesenchymal stem/stromal cell conditioned media as a long-lasting treatment for pain and psychiatric comorbidities in a murine model of osteoarthritis

Giada Amodeo [a,1], Stefania Niada [b,1], Giulia Galimberti [a], Silvia Franchi [a], Elena Della Morte [b], Michela Taiana [c], Simona Piccolo [c], Stefania Ceruti [a], Laura de Girolamo [c], Anna Teresa Brini [b,d,2], Paola Sacerdote [a,2,*]

[a] Pain Therapy and Neuroimmunology Unit, Department of Pharmacological and Biomolecular Sciences "Rodolfo Paoletti", Università degli Studi di Milano, Milan, Italy
[b] Laboratory of Biotechnological Applications, IRCCS Istituto Ortopedico Galeazzi, Milan, Italy
[c] Orthopaedic Biotechnology Laboratory, IRCCS Istituto Ortopedico Galeazzi, Milan, Italy
[d] One Health Unit, Department of Biomedical, Surgical and Dental Sciences, Università degli Studi di Milano, Milan, Italy

ARTICLE INFO

Keywords:
Mesenchymal stem/ stromal cell secretome
Mesenchymal stem/ stromal cell conditioned medium
Mesenchymal stromal cells priming
Osteoarthritis murine model
Pain
Neuroinflammation
Anxiety-like behavior
Depression-like behavior
Mood alterations

ABSTRACT

Osteoarthritis (OA) is a prevalent musculoskeletal condition characterized by chronic pain and often accompanied by psychiatric comorbidities, such as anxiety and depression. The mesenchymal/stromal cell (MSC) secretome has emerged as promising therapy due to its immunomodulatory and regenerative properties. This study aimed to compare the therapeutic efficacy of standard (CM) and cytokine-primed conditioned media (CM^+) derived from human adipose-derived MSCs in mitigating pain, mood alterations and neuroinflammation in a murine OA model. OA was induced by intra-articular injection of monoiodoacetate in male C57BL/6J mice. On day 7, mice received a single intravenous dose of CM or CM^+ at two concentrations. Pain-related behavior was assessed by mechanical and thermal nociceptive tests. Anxiety- and depression-like behaviors were evaluated through open field, light/dark box, and forced swim tests. Pro- and anti-inflammatory cytokines and (neuro) inflammatory markers were analyzed in OA joint, and in the peripheral and central nervous system. Peripheral innervation and substance P were assessed in OA paw skin. Both CM and CM^+ reduced painful and affective symptoms in a dose-dependent manner. However, CM (from non-primed MSCs) exhibited faster onset and longer-lasting effects, up to 17 days post-injection, compared to CM^+.

CM also led to greater improvements in neuroinflammatory profiles, rebalancing cytokine pattern and macrophage polarization across peripheral and central tissues. MSC secretome, especially when generated without inflammatory priming, represents a safe and long-lasting therapeutic option for OA pain and associated mood disorders. These findings highlight its clinical potential as an innovative multi-targeted biological therapy.

1. Introduction

Osteoarthritis (OA) is a chronic, degenerative joint disease and the leading cause of musculoskeletal pain worldwide. It is characterized by progressive cartilage degradation, subchondral bone remodeling, synovial inflammation, and osteophyte formation (Tong et al., 2022). While structural changes in the joint are central to OA, pain is the most prominent and disabling symptom, often leading to reduced mobility, decreased quality of life, and increased healthcare utilization. The mechanisms underlying OA pain are complex and multifactorial, involving peripheral nociceptive input from joint tissues as well as central sensitization processes. Despite its high prevalence and burden, current treatments are largely palliative, with limited options for effectively managing chronic OA pain (El-Tallawy et al., 2021; Johnson and Hunter, 2014). Moreover, anxiety, depression and sleep disturbances are also present (Axford et al., 2010; Goldenberg, 2010; Sharma

* Corresponding author.
E-mail address: paola.sacerdote@unimi.it (P. Sacerdote).
[1] These authors contributed equally as first author.
[2] These authors contributed equally as last authors.

https://doi.org/10.1016/j.bbi.2026.106297
Received 14 October 2025; Received in revised form 14 January 2026; Accepted 18 January 2026
Available online 20 January 2026

et al., 2016), impacting the patient's quality of life and further aggravating pain perception, leading to the establishment of a self-perpetuating vicious circle (Moriarty and Finn, 2014; Moriarty et al., 2011). Novel efficacious approaches are needed.

Mesenchymal stem/stromal cells (MSCs) possess important immunomodulatory and pro-regenerative properties, making them suitable candidates for the treatment of chronic pain and inflammation. Accordingly, in recent years, MSC effect on pain has been investigated in various clinical fields, including migraine, low back pain, disk degeneration and osteoarthritis (Supplementary Table 1). It is now largely accepted that MSCs exert their therapeutic effects through paracrine action. Indeed, the MSC secretome, defined as the set of MSC-derived bioactive factors (proteins, nucleic acids and lipids) delivered either in extracellular vesicles (EVs) or in a free form, has shown therapeutic effects similar to those observed after MSC transplantation (Brini et al., 2017). Moreover, secretome use presents important advantages, such as easier storage, the possibility of producing large batches of allogeneic conditioned medium (CM) ready for use, and the ability to cross biological barriers. Recently, the MSC whole secretome and its extracellular vesicles have been investigated for multiple conditions, including osteoarthritis, ulcers, COVID-19 infection, and graft-versus-host disease (Supplementary Tables 2 and 3). Notably, the MSC secretome can be modified by conditioning or priming the donor cells. This can be achieved by either treating donor cells with cytokines, drugs chemical agents, or applying different culture conditions, hypoxia, or selected biomaterials (Noronha et al., 2019). Inflammatory cytokine priming has been used to modulate MSCs and their secretome, aiming to develop more effective therapeutic agents for osteoarthritis (Barrachina et al., 2018; Jammes et al., 2023; Ragni et al., 2020) and pain (Liu et al., 2021). Recently, we selected a priming protocol based on a 5-minute stimulation of adipose-derived mesenchymal stem/stromal cells (ASCs) with TNFα and IL-1β, significantly enriching ASC-CM in proteins, vesicles, and immunomodulatory factors (Giannasi et al., 2024).

We previously demonstrated that intravenously injected ASC-CM was able to reduce pain and neuroinflammation in the monoiodoacetate (MIA) murine model of osteoarthritis (Amodeo et al., 2021a). However, a direct comparison of standard and primed secretome (CM/CM$^+$) in MIA pain model was never performed.

Moreover, psychiatric comorbidities often coexist with chronic pain, and a high incidence of anxiety and depression is reported in OA patients. Different studies suggested that the underlying mechanisms involved in chronic pain processes are also implicated in psychiatric disorders due to a neurobiological overlap between pain processing and emotional signals (Zhuo, 2016). Particularly, a pivotal role for neuroinflammation in the central (CNS) and peripheral nervous system (PNS) in the pathogenesis of both chronic pain and depressive/anxious diseases is now recognized (Amodeo et al., 2023; Amodeo et al., 2024; Amodeo et al., 2021b; Barcelon et al., 2019; Geraghty et al., 2021; Ji et al., 2018; Matsuda et al., 2019; Zhuo, 2016). We and others consistently demonstrated the co-presence of pain, anxiety, depression and neuroinflammatory condition in PNS and CNS in the MIA model. It is therefore important to understand the underlying mechanisms to develop innovative treatments that can simultaneously control the nociceptive and affective manifestations of OA. In this work, we analyze and compare the efficacy of CM and CM$^+$ in relieving pain, psychiatric comorbidities and neuroinflammation in the MIA murine model.

2. Materials and methods

2.1. Adipose-derived mesenchymal stem/stromal cells (ASCs) isolation and culture

ASCs were obtained from waste subcutaneous adipose tissues of six patients undergoing total hip replacement surgery (patient details in Supplementary Table 4) collected at IRCCS Ospedale Galeazzi Sant'Ambrogio, with patient-informed consent and ethical approval (TENET–IRCCS Ospedale San Raffaele ethics committee, approval number 38/int/2022). Cells were isolated and cultured as previously described (Amodeo et al., 2021a; Niada et al., 2021). Briefly, adipose tissue was enzymatically digested with 0.75 mg/ml type I collagenase (Worthington Biochemical Corporation, Lakewood, NJ, USA) for 30 min, followed by filtration through a 100-μm cell strainer (Corning Incorporated, Corning, NY, USA). The isolated cells were then cultured at a density of 10^4 cells/cm^2 in high-glucose DMEM supplemented with 10% FBS (Euroclone, Pero, Italy), 2 mM L-glutamine, 50 U/ml penicillin, and 50 μg/ml streptomycin. Cultures were maintained at 37 °C in a humidified atmosphere with 5% CO_2. Cells were characterized as indicated in Supplementary Fig. 1.

2.2. Cell priming and CM production

ASCs at passages IV to VI were used for the experiments. Priming was induced as previously published (Giannasi et al., 2024). Briefly, upon reaching confluence, ASCs were rinsed with PBS and either stimulated with 10 ng/ml TNFα and10 ng/ml IL-1β for 5 min or left unstimulated. Cells were then rinsed twice with PBS and maintained in serum-free conditions for 72 h. Afterward, cells were detached and counted to correlate their number with secretome volume. Conditioned medium (CM) and primed conditioned medium (CM$^+$) were collected and centrifuged at 2500*g for 10 min at 4 °C to remove dead cells and debris. The supernatants were further centrifuged at 3850*g for 110 min at 4 °C using Amicon Ultra-15 centrifugal filter devices (3 kDa cut-off; Merck Millipore, Burlington, MA, USA), then aliquoted and stored at −80 °C. Protein content was quantified using the Bradford assay (PerkinElmer, Milan, Italy). Pooled CM and CM$^+$ samples were derived from 48.1 x 10^6 and 49.2 x 10^6 ASCs, respectively, and stored at −80 °C. At the time of in vivo treatment, CM was thawed and the amount corresponding to CM derived from 1 or 2 million cells was administered to each mouse.

2.3. Western blotting of standard and primed ASCs

After CM production, ASC and primed ASC (ASC$^+$) were lysed in 50 mM Tris-HCl (pH 7.5), 150 mM NaCl, 1% NP-40, and 0.1% SDS, supplemented with a protease inhibitor cocktail (PIC) and 2 mM PMSF. Lysates were incubated on ice for 30 min, subjected to three freeze–thaw cycles, and centrifuged at 14,000*g for 10 min at 4 °C. Supernatants were collected and stored at − 20 °C until use. Protein content was quantified using the BCA assay (Thermo Fisher Scientific, Waltham, MA, USA), and 10 μg of protein per sample was analyzed by 10% SDS-PAGE and Western blotting following standard protocols. Primary antibodies against Cyclooxygenase-2 (rabbit anti-COX2; #12282, Cell Signaling, Danvers, MA, USA; 1:1000), Indoleamine 2,3-dioxygenase (rabbit anti-IDO; #86630, Cell Signaling; 1:1000), and β-actin (mouse anti-β-actin; A2228, Merck, Darmstadt, Germany; 1:5000) were incubated overnight at 4 °C or for 1 h at room temperature for the housekeeping β-actin (ACTB). Specific signals were detected using appropriate horseradish peroxidase-conjugated secondary antibodies and visualized with ECL Westar Supernova (Cyanagen, Bologna, Italy). Signal acquisition was performed using a ChemiDoc Imaging System (Bio-Rad, Milan, Italy), and densitometry analysis was conducted with Image Lab Software version 6.1 (Bio-Rad). Protein expression was normalized on the corresponding loading control (ACTB). Fold change was calculated by normalizing protein expression in each sample to the control sample (ASC = 1).

2.4. Secretome Characterization

Protein concentration was measured by the Bradford assay (Bio-Rad Laboratories, Hercules, CA, USA). Nanoparticle tracking analysis, flow cytometry and Western blotting were used to characterize the extracellular vesicles included in the CM, as previously described (Giannasi et al., 2020), as detailed below.

2.4.1. Nanoparticle tracking analysis (NTA)

CM and CM^+ pools were diluted in 0.22 μm triple-filtered PBS and analyzed using a NanoSight NS300 (Malvern PANalytical, Salisbury, UK). For each sample, three 1-minute videos were recorded, ensuring quality criteria of 20–120 particles per frame, particle concentrations between 10^6 and 4 x 10^9 particles/ml, and valid tracks exceeding 20%. Video analysis was performed using the built-in NanoSight Software NTA.

2.4.2. Flow cytometry

Prior to cytofluorimetric analysis, CM and CM^+ pools were diluted 1:10 and 1:20, respectively, in 0.22 μm triple-filtered PBS and stained with the green fluorescent dye CFSE-DA (carboxyfluorescein diacetate succinimidyl ester, Biotium, Fremont, CA, USA). Specifically, ASC-CM/CM + were incubated with 20 nM CFSE for 1 h at 37 °C and analyzed without further washing. Data acquisition was performed using a CytoFLEX flow cytometer (Beckman Coulter, Brea, CA, USA). Instrument calibration was set using a Megamix-Plus SSC and FSC mix (Biocytex, Marseille, France), a reference bead mixture containing FITC-conjugated fluorescent spheres of varying sizes (100 nm, 160 nm, 200 nm, 240 nm, 300 nm, 500 nm, and 900 nm). CFSE-positive ($CFSE^+$) ASC-CM was analyzed in the Violet SSC-H and FITC-H channels, with event regions defined according to standardization bead coordinates (Supplementary Fig. 2). $CFSE^+$ samples were then aliquoted and incubated for 30 min at 4 °C in the dark with APC-conjugated antibodies against CD9, CD63, and CD81 (BioLegend, San Diego, CA, USA; 1:20 dilution). Samples were diluted to a final volume of 300 μl in 0.22 μm triple-filtered PBS, and 50,000 events were acquired at a medium flow rate. DMEM-diluted antibodies and unlabeled samples were used as controls.

2.4.3. Luminex discovery assay

The levels of specific molecules in CM and CM^+ were evaluated using the Human Premixed Multi-Analyte Kit LXSAHM (R&D Systems, Minneapolis, MN, USA), following the manufacturer's standard protocols. The kit was customized to quantify the concentrations of CCL2, CCL3, CXCL1, M−CSF, G-CSF, IFNγ, IL-8, IL-10, IL-4, IL-1RA, TIMP-1, HGF, OPG, and VEGF-A. Samples were appropriately diluted (1:2, 1:500, or 1:5000) and analyzed using the Bio-Plex Multiplex System (Bio-Rad, Milan, Italy). Data acquisition and analysis were conducted using MAGPIX PONENT 4.2 software (Luminex Corporation, Austin, TX, USA).

2.5. Animals

Ten-week-old C57BL/6J male mice (n = 36, Charles River Laboratories, Italy) were used. Animals were housed, 3 per cage (type II – 26 x 20 x 14 cm), in a SPF animal facility with monitoring of dark/light cycle (lights-on: 7:00 a.m.; light-off: 7:00p.m.), room temperature (22 ± 1 °C) and humidity (55 ± 10%). Each cage was outfitted with bedding, nesting material and environmental enrichment. Free access to standard pellets and tap water was provided. Before starting the experiments, mice were acclimated for 1 week and accustomed to handling by experimenters involved (few minutes daily). Additionally, periodic veterinary checks were conducted to assess the well-being of mice. The experimental protocol flowchart is reported in Fig. 1.

The ARRIVE guidelines and 3R principles were followed. All procedures were conducted in accordance with EU Directive 2010/63 and approved by the Committee for the Care and Use of Animals of the Italian Ministry of Health (authorization number 180/2020 to PS).

2.6. Osteoarthritis induction

As previously described (Amodeo et al., 2022; Galimberti et al., 2023), under general anesthesia, OA was induced by a single intra-articular administration into the right knee with 1 mg of MIA (Sigma-Aldrich, Italy) in 10 μl of sterile saline (MIA group, n = 30). Control mice were treated with vehicle (CTR group, n = 6). Randomization in experimental groups was performed by the online source GraphPad (Amodeo et al., 2025).

2.7. Therapeutic treatment

On day 7 post-OA induction, MIA mice were randomized (see above) into 5 experimental groups for therapeutic treatment with CM or CM^+. Both CMs were injected into mice by intravenous injection (tail vein, final volume 200 μl) at two different doses: conditioned media from 1 x 10^6 ASC (CM1 and $CM1^+$ group, respectively) and 2 x 10^6 ASC (CM2 and $CM2^+$ group, respectively). A group of MIA mice was treated with vehicle alone. Each group consisted of 6 mice.

2.8. Behavioral tests

Before each behavioral test session, mice were acclimatized in the new room for about 30 min. Tests were performed from least to most impactful/stressful. Between the tests, mice were relocated in the home cage and allowed to rest for an adequate period. Tests were performed in the light phase, always in the morning, by researchers who were blind to

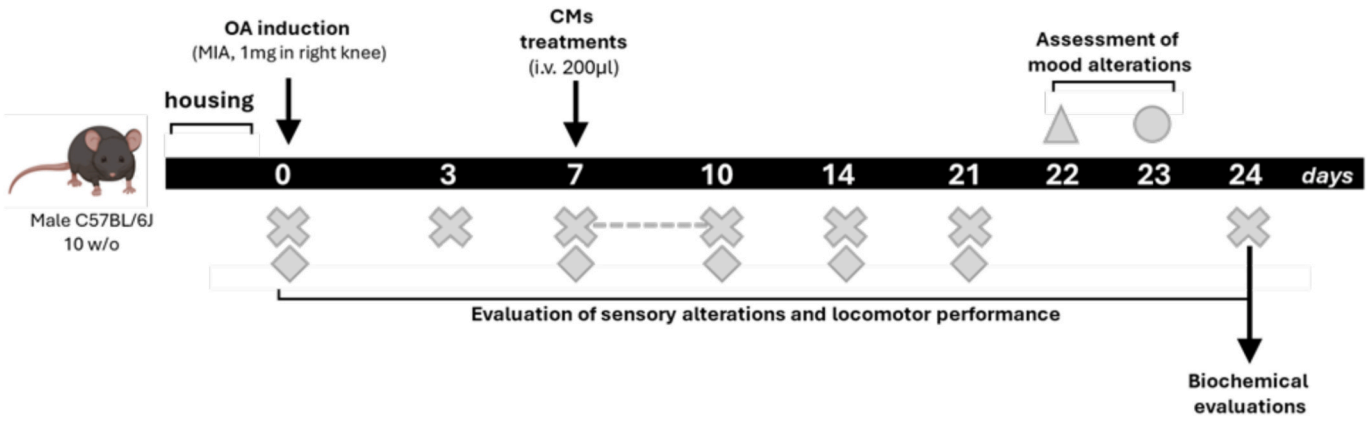

Fig. 1. Experimental protocol. (X) Pain like-behavior evaluations (mechanical allodynia by von Frey test and thermal hyperalgesia by plantar test). (−—) Pain-like behavior evaluations after 1 and 3 h and 2 days from treatments. (◆) Locomotor performance assessment (gait alterations by limping test, changes in endurance and balance by rotarod test and variations in muscle strength with grip strength meter test). (▲) Assessment of anxiety-like behavior (open field test and light/dark box tests). (●) Assessment of depressive-like behavior (forced swim test).

all experimental conditions.

2.8.1. Pain-like behavior tests

Nociceptive assessments were performed before (day 0, baseline) and 3, 7, 9, 10, 14, 21 and 24 days after OA induction, by the von Frey test (mechanical allodynia) and plantar test (thermal hyperalgesia). Additionally, on day 7 post-MIA, mice were tested with von Frey test also after 1 and 3 h from treatment with CMs to check for any acute effects. In both tests, the ipsilateral paw (saline or MIA injection in the respective knee) and contralateral paw (without injection) were tested (3 measurements/paw). Since no nociceptive changes were observed on the contralateral paw, only the mean value obtained from the ipsilateral paw was calculated and used for statistical analysis (Amodeo et al., 2022; Amodeo et al., 2025; Amodeo et al., 2021a; Brini et al., 2017; Galimberti et al., 2023).

i) von Frey test: mechanical allodynia was evaluated by dynamic plantar aesthesiometer (Model 37,550 – Ugo Basile, Italy), as previously reported (Amodeo et al., 2025). Briefly, a blunt probe (von Frey filament, Ø 0.5 mm, ranging up to 10 g-(g) in 10 s-(s)) was applied on the hind-paw central plantar surface. The test ended when the animal removed its paw or when the cut-off (10 g) was reached. Responses to mechanical stimuli were reported as paw withdrawal thresholds (PWT, expressed in g).

ii) Plantar test: thermal hyperalgesia was tested using a Hargreaves apparatus (Model 37,570 – Ugo Basile, Italy), as previously reported (Amodeo et al., 2025). Briefly, a constant radiant intensity heat beam (Ø 0.5 cm, Ω 20 IR) was applied to the mid-plantar area of hind paws. Test ended when the animal removed its paw or when the cut-off (22 s) was reached. Responses to thermal stimuli were reported as paw withdrawal latency (PWL, expressed in s).

2.8.2. Motor behavior tests

Changes in gait, balance and coordination, and muscle strength were assessed before (day 0, baseline) and after 7, 10, 14, and 21 days after OA induction.

i) Gait alternations: limping was assessed by observing the animal left free to move within a plexiglass arena for 60 s, as previously reported (Amodeo et al., 2021a). Animal's behavior was assessed, looking at the ipsilateral (right) leg, according to the following point scale: 5 – normal gait, 4 – rapid limping/dragging, 3 – repeated limping or prolonged dragging, 2 – repeated limping associated with evident dragging, 1 – constant dragging and limping. For each mouse, scores assigned by at least three researchers were averaged and used for statistical analysis.

ii) Rotarod test: before the first session, mice were adequately trained on the apparatus (Model 47,650 – Ugo Basile, Italy), as previously described (Amodeo et al., 2022). To evaluate endurance and balance, each animal was tested three times with 15-minute intervals between tests with an acceleration protocol (10–50 rpm in 300 sec). Test ended when the cut-off (300 s) was reached, when the animal fell from the rod or if during the test the animal remained on the rod but performed 3 consecutive passive rotations. For each mouse, the mean time of the baseline performance (day 0) was subtracted from the average time of the subsequent performances and used for statistical analysis.

iii) Grip strength meter test: it was used to measure the muscle strength of all four limbs (Model 47,200 – Ugo Basile, Italy), as previously described (Amodeo et al., 2022). Evaluation was repeated 3 consecutive times for each animal and the apparatus automatically detected the mice response (force range: 0.1–1500 g). Values obtained were averaged and used for statistical analysis.

2.8.3. Anxiety- and depressive-like behavior

Tests were evaluated at the end of the experimental protocol (22 and 23 days after OA induction, respectively) through the Open Field (OF) test and Light/Dark Box (LDB) test (for anxiety) and Forced Swim (FS) test (for depression). All mood alteration tests were recorded and analyzed with the video tracking software ANY-maze (v 7.1) (Amodeo et al., 2023; Amodeo et al., 2025; Amodeo et al., 2021b; Galimberti et al., 2023).

i) OF test: as previously described (Amodeo et al., 2023), mouse was placed in the middle of the apparatus (Model 47150-Ugo Basile, Italy) and allowed to roam around freely for 10 min(−min). The total distance travelled in the arena; the total time spent in the center zone and the number of transitions in the center zone were used for statistical analysis.

ii) LDB test: as previously described (Amodeo et al., 2023; Amodeo et al., 2021b), the mouse was put in the white chamber of the apparatus (Model 47,445 – Ugo Basile, Italy) and allowed to freely move between the two chambers for 5 min. The latency (i.e. the consecutive time spent in the dark room before returning to the light room for the first time), the total time spent in the white chamber and the transitions between chambers were used for statistical analysis.

iii) FS test: as previously described (Amodeo et al., 2023; Amodeo et al., 2021b), a glass beaker full of water (h 27 cm, Ø 14.5 cm, water temperature 23 ± 2 °C) was used as apparatus, in which the mouse was gently placed and allowed to swim undisturbed for 6 min. After this period, the animal was removed, dried and returned to its home cage. The latency (i.e. the first moment of prolonged immobility ≥ 10 s) and the total immobility time during both the first 2 min (realization time) and the last 4 min (test time) of the test were used for statistical analysis.

2.9. Tissue collection

On day 24 post-OA induction, i.e. 17 days after the treatment with CMs, mice were sacrificed by decapitation. Ipsilateral hind paw footpad skin biopsies, ipsilateral knee, ipsilateral sciatic nerve and its distal branches (tibial, common peroneal and sural nerves), ipsilateral dorsal root ganglia (DRG,L3-L6), spinal cord (L3-L6) and brain areas (prefrontal cortex and hippocampus), were isolated and immediately processed (paw skin) or snap frozen in liquid nitrogen and stored at − 80 °C for following biochemical analysis.

2.10. RT-qPCR

Total RNA was extracted from tissue through an ultrasonic processor (UP50H DR. Hielscher, Germany) and TRIzol® reagent (Invitrogen, USA) according to the manufacturer's instructions. Complementary DNA (cDNA) was synthesized using the LunaScript™ Reverse Transcriptase Kit (New England BioLabs, UK The mRNA expression levels of the selected genes were quantified by real-time PCR using the StepOnePlus™ Real-Time PCR System (Applied Biosystems™, Italy), Luna® Universal Probe qPCR Master Mix (New England BioLabs, UK), and specific TaqMan™ Gene Expression Assays (FAM, Applied Biosystems™). The analyzed genes included pro-inflammatory cytokines Interleukin 1 beta (IL-1β, Mm00434228_m1), Interleukin 6 (IL-6, Mm00446190_m1) and Tumor Necrosis Factor alpha (TNFα, Mm00443258_m1), and the anti-inflammatory cytokine Interleukin 10 (IL-10, Mm00439616_m1). To assess macrophage and microglial activation, we measured the expression of macrophage/microglial markers Cluster of Differentiation 68 (CD68, Mm03047343_m1), Cluster of Differentiation 11b (CD11b, Mm00434455_m1) and Ionized calcium-binding adapter molecule 1 (Iba1, Mm00479862_g1). Markers of specific activation phenotypes were also included: Cluster of Differentiation 86 (CD86, Mm00444540_m1) for the pro-inflammatory phenotype and Cluster of Differentiation 206 (CD206, Mm01329359_m1) for the anti-inflammatory phenotype. The Glial Fibrillary Acidic Protein (GFAP, Mm01253033_m1) was used as a marker of Schwann cells in the sciatic nerve, satellite glial cells in the dorsal root ganglia (DRG) and astrocytic cells in brain regions. Activating Transcription Factor 3 (ATF3, Mm00476033_m1) was analyzed as a marker of cellular stress and neuronal damage, Calcitonin Gene-Related Peptide (CGRP, Mm00801463_g1) as a neurogenic mediator and Doublecortin (DCX,

Mm00438400_m1) as a marker of neurogenesis. mRNA levels were normalized on those of the endogenous gene GlycerAldehyde 3-Phosphate DeHydrogenase (GAPDH, Mm99999915_g1) and expressed as 2^(−ΔΔCt) relative to CTR group. Each sample was run in triplicate together with non-template controls (NTC).

2.11. Western blotting (DRG)

Proteins from DRG were collected using TRIzol reagent (R) (Invitrogen, USA), following manufacturer protocol. Protein content was quantified using the BCA assay (Thermo Fisher Scientific, Waltham, MA, USA). Ten μg of proteins per sample were resolved in 12% SDS-PAGE. Western blotting was conducted with antibodies against GFAP (sc-33673, Santa Cruz Biotechnology, Dallas, USA, 1:200), Iba1/AIF-1 (#17198, CST, 1:500) and β-actin (A2228, Merck, Darmstadt, Germany, 1:5000). Specific signals were detected as described above. Protein expression was normalized on the corresponding loading control (ACTB). Fold change was calculated by normalizing each sample's expression to the control sample.

2.12. Immunofluorescence

Skin biopsies from affected hind paw were collected using a 3 mm round punch. Samples were fixed in 2% paraformaldehyde–lysine–periodate for 24 h at 4 °C, followed by overnight cryoprotection. Tissue sections (20 μm) were obtained using a cryostat (Bio-Optica, Italy). Two to five sections per sample were randomly selected for free-floating immunostaining with primary antibodies against the general nerve marker protein gene product 9.5 (mouse-anti PGP 9.5, 1:1000, #MCA4750GA, Bio-Rad, Italy) and the sensory neuropeptides substance P (rabbit anti-SP, 1:600, #20064, ImmunoStar, Hudson, USA). Secondary antibodies (1:1000, AlexaFluor 488 or 647, Invitrogen, USA) were then applied and sections were mounted with DAPI-containing mounting medium. Fluorescence images were acquired using a Leica TCS-SP8 confocal microscope with sequential acquisition at 60X magnification. For intraepidermal nerve fiber density (IENFD) quantification, PGP 9.5-positive IENFs crossing the dermal–epidermal junction were counted, excluding secondary branching within the epidermis, and normalized to total epidermal length to calculate linear IENF density (Sassone et al., 2016). For SP evaluation, three to five fields per section were analyzed. The immunoreactive area of SP was quantified relative to the total PGP 9.5 fiber area using ImageJ software (Facer et al., 2007).

2.13. Statistical analysis

Statistical analyses were performed using GraphPad Prism 10 (v3, USA) by investigators blind to treatments. Data distribution was assessed by the Shapiro–Wilk test. Specifically, unpaired *t*-test was used to analyze standard ASC and preconditioned ones (ASC^+) together with CM and CM^+ features (Fig. 1). For ASC and ASC^+ comparison, data represent mean ± SEM of 4 populations; for CM and CM^+ content, data represent mean ± SEM of 8 CM batches. Behavioral tests were analyzed by two-way ANOVA followed by Bonferroni's post hoc test (Fig. 2) and biochemical evaluations were analyzed by one-way ANOVA followed by Tukey's post hoc test (Figs. 3–5). Immunofluorescent data represent mean ± SEM of 5–6 mice/group, qPCR data represent mean ± SEM of 6 mice/group and WB data represent mean ± SEM of 5 mice/group. No animal or data were excluded. For all analyses, differences were considered significant at $p \leq 0.05$. Detailed statistical analysis is provided in Supplementary Tables 5 and 6.

3. Results

3.1. ASC activation and secretome modulation by inflammatory cytokine priming

Inflammatory cytokine priming induced sustained ASC activation, which persisted throughout the three-day medium conditioning period, as evidenced by increased expression of COX-2 and IDO (Fig. 2A-B, respectively). The stimulation also enhanced the total protein content of the ASC-CM (Fig. 2C and Supplementary Table 7) and the release of specific factors involved in immune cells recruitment and modulation (e.g., CCL2, CCL3, IL-8) and in tissue regeneration (e.g., HGF and VEGF-A) (Fig. 2E). Consistently, the number of particles increased (Fig. 2D), while the expression of EV markers remained unchanged (Fig. 2F-K and Supplementary Fig. 3).

3.2. CM relieves pain and mood alterations more efficaciously than CM^+

As expected, OA mice exhibited significant mechanical allodynia and thermal hyperalgesia (Fig. 3A-B). Both CM and CM^+ significantly counteracted both mechanical allodynia and thermal hyperalgesia in a dose–response fashion. The anti-hypersensitivity effect of CM1 and $CM1^+$ was lower than that of CM2 and $CM2^+$. However, some differences were present between CM2 and $CM2^+$: the effect of CM2 was faster than $CM2^+$, showing significant inhibition of hypersensitivities already 1-h after administration, while $CM2^+$ effects on thermal hyperalgesia appeared only two days later. Moreover, the antiallodynic and anti-hyperalgesic effects of CM2 were always significantly higher than those exerted by $CM2^+$, and they remained maximal up to 17 days after administration, in contrast to what was observed in $CM2^+$-treated mice, where they began to decline at this time point. Both CM2 and $CM2^+$ reduced limping (Fig. 3C) and ameliorated locomotor activity (Fig. 3D) while only CM2 improved grip strength (Fig. 3E). Similar to results on pain, CM2 exerted a more robust effect than the $CM2^+$. Both CM1 and $CM1^+$ were not effective on these parameters. We then checked the presence of mood alterations 22–23 days after MIA injection, corresponding to 15–16 days from CM and CM^+ treatments. Anxiety-like behavior, evaluated with the OF (Fig. 3F-H) and LDB (Fig. 3I-K) tests, was observed in OA mice. A decreased number of entries and reduced time spent in the center zone of the OF were observed. In the LDB test prolonged latency to return from the dark to the light room, reduced time in the white chamber and fewer chamber transitions were registered. Parallel to what observed for pain, both CM2 and $CM2^+$ significantly counteracted anxiety-like behavior development in OA mice, with only minor differences between them. Conversely, both CM1 and $CM1^+$ were less efficacious in contrasting anxiety-like behavior. MIA mice were also characterized by depressive-like behavior (Fig. 3L-N), as demonstrated by lower latency and longer immobility time (4 min) in the FS test. CM2 treatment ameliorated depressive behavior, and again the effect was more evident than that observed after $CM2^+$. CM1 and $CM1^+$ were not effective on depressive-like behaviors.

3.3. CM2 controls paw skin and knee inflammatory markers

Based on their efficacy in behavioral tests, we decided to perform biochemical evaluations only in tissues from mice treated with CM2 and $CM2^+$. Chronic pain can be associated with reduced skin innervation, measured as expression of Protein Gene Product 9.5 (PGP 9.5) in axons of the epidermis and dermis. However, as reported in Fig. 4A-B, we did not observe alterations of the $PGP9.5^+$ nervous fiber density in the paw skin of any group. SP was significantly elevated in PGP 9.5 co-labeled fibers in the paw skin from OA mice, suggesting neurogenic inflammation, and both CM2 and $CM2^+$ were able to significantly reduce its upregulation (Fig. 4A and 4C). As shown in Fig. 4D-M, MIA mice are characterized by an overt inflammatory condition in the OA knee joint. mRNA expression levels of the pro-inflammatory cytokines IL-1β, IL-6

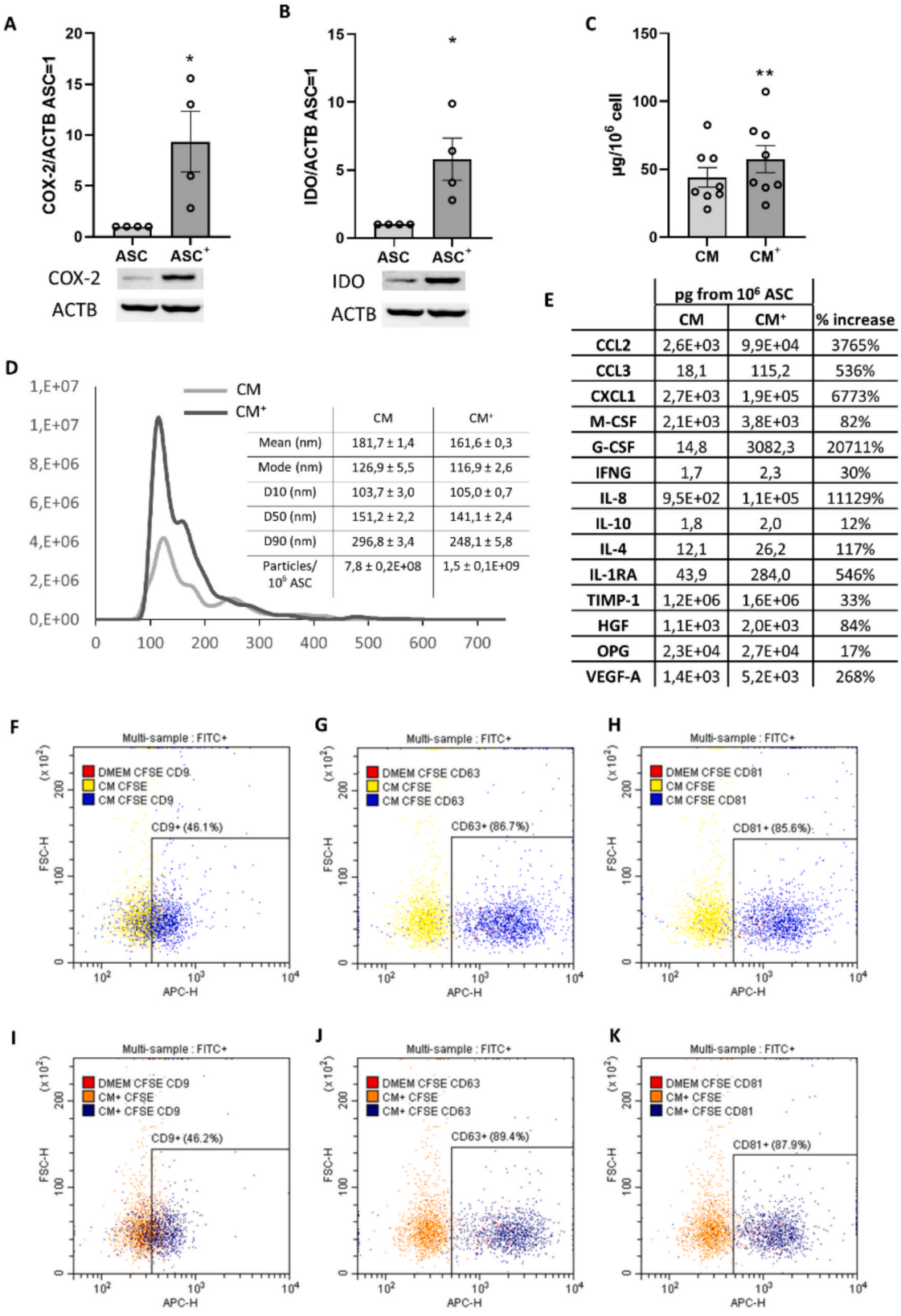

	pg from 10^6 ASC		
	CM	CM+	% increase
CCL2	2,6E+03	9,9E+04	3765%
CCL3	18,1	115,2	536%
CXCL1	2,7E+03	1,9E+05	6773%
M-CSF	2,1E+03	3,8E+03	82%
G-CSF	14,8	3082,3	20711%
IFNG	1,7	2,3	30%
IL-8	9,5E+02	1,1E+05	11129%
IL-10	1,8	2,0	12%
IL-4	12,1	26,2	117%
IL-1RA	43,9	284,0	546%
TIMP-1	1,2E+06	1,6E+06	33%
HGF	1,1E+03	2,0E+03	84%
OPG	2,3E+04	2,7E+04	17%
VEGF-A	1,4E+03	5,2E+03	268%

Fig. 2. ASC/ASC$^+$ and CM/ CM$^+$ features. Expression of COX-2 (**A**) and IDO (**B**) in ASC and ASC$^+$, at the time of collection of secretome, analyzed by Western blotting. Specific bands were quantified through Image Lab Software v 6.1 (Bio-Rad, Milan, Italy), and data (n = 4) were normalized on ACTB and expressed as relative values (ASC = 1). Representative blots are shown below. (**C**) Total protein content of CM and CM$^+$. Data (n = 8) are expressed as mean ± SEM. (**D**) Nanoparticle Tracking Analysis (NTA) of CM and CM$^+$ pools; the table shows the dimensional parameters of the samples expressed as mean ± SD of 3 technical replicates. (**E**) Levels (pg/10^6 ASC) of selected proteins in CM and CM$^+$ identified through Bio-Plex Multiplex System, with relative changes expressed as percentage increase. (**F, I**) CD9, (**G, J**) CD63, and (**H, K**) CD81 staining of CM and CM$^+$ pools. Statistical analyses were performed by paired Student's *t* test. *p < 0.05 vs. ASC, **p < 0.01 vs. CM.

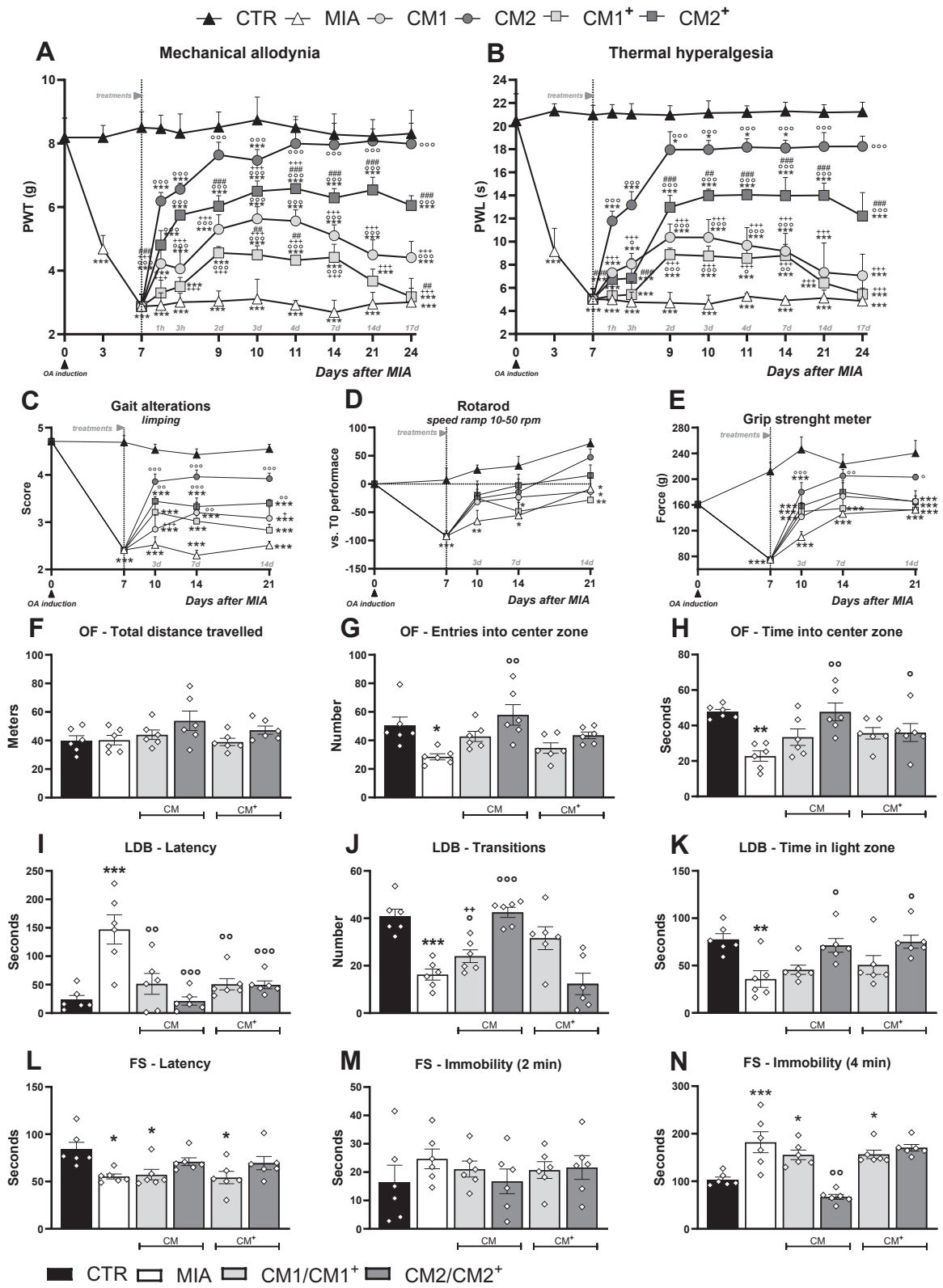

Fig. 3. Behavioral tests. Osteoarthritis (OA) was induced at day 0 and after 7 days, mice were treated with 2 different conditioned medium (CM and CM$^+$) both at two doses (CM1/CM2, CM1$^+$/CM2$^+$). Pain-like behavior, i.e. (**A**)-mechanical allodynia and (**B**)-thermal hyperalgesia as well as motor performance, i.e. (**C**)-gait alterations, (**D**)-endurance and balance, and (**E**)-muscle strength, were evaluated. Anxious-like behavior was assessed by open field-(OF) test, evaluating (**F**) total distance traveled, (**G**) number of entries (**H**) and time spent in central area, and by the light/dark box-(LDB) test evaluating (**I**) first latency to exit the dark zone, (**J**) transition and (**K**) time spent in the light zone as well as depressive-like behavior by the forced swim-(FS) test evaluating (**L**) latency, i.e. first immobility $\geq$ 10 s, (**M**) immobility time in first 2 min and (**N**) in last 4 min of the test. Hours-(h) and days-(d), in grey, identify the time after treatments. PWT and PWL indicate paw or latency withdrawal threshold, respectively. Results are expressed as mean $\pm$ SEM of 6 mice/group. Statistical analysis was performed by Two- (A-E) or One- (F-N) way ANOVA followed by Bonferroni post test. *$p < 0.05$, **$p < 0.01$, ***$p < 0.001$ vs. CTR; °$p < 0.05$, °°$p < 0.01$, °°°$p < 0.001$ vs. MIA; +$p < 0.05$, ++$p < 0.01$, +++$p < 0.001$ vs. same conditioning strategy at higher dose; ##$p < 0.01$, ###$p < 0.001$ vs. same-dose conditioning strategy.

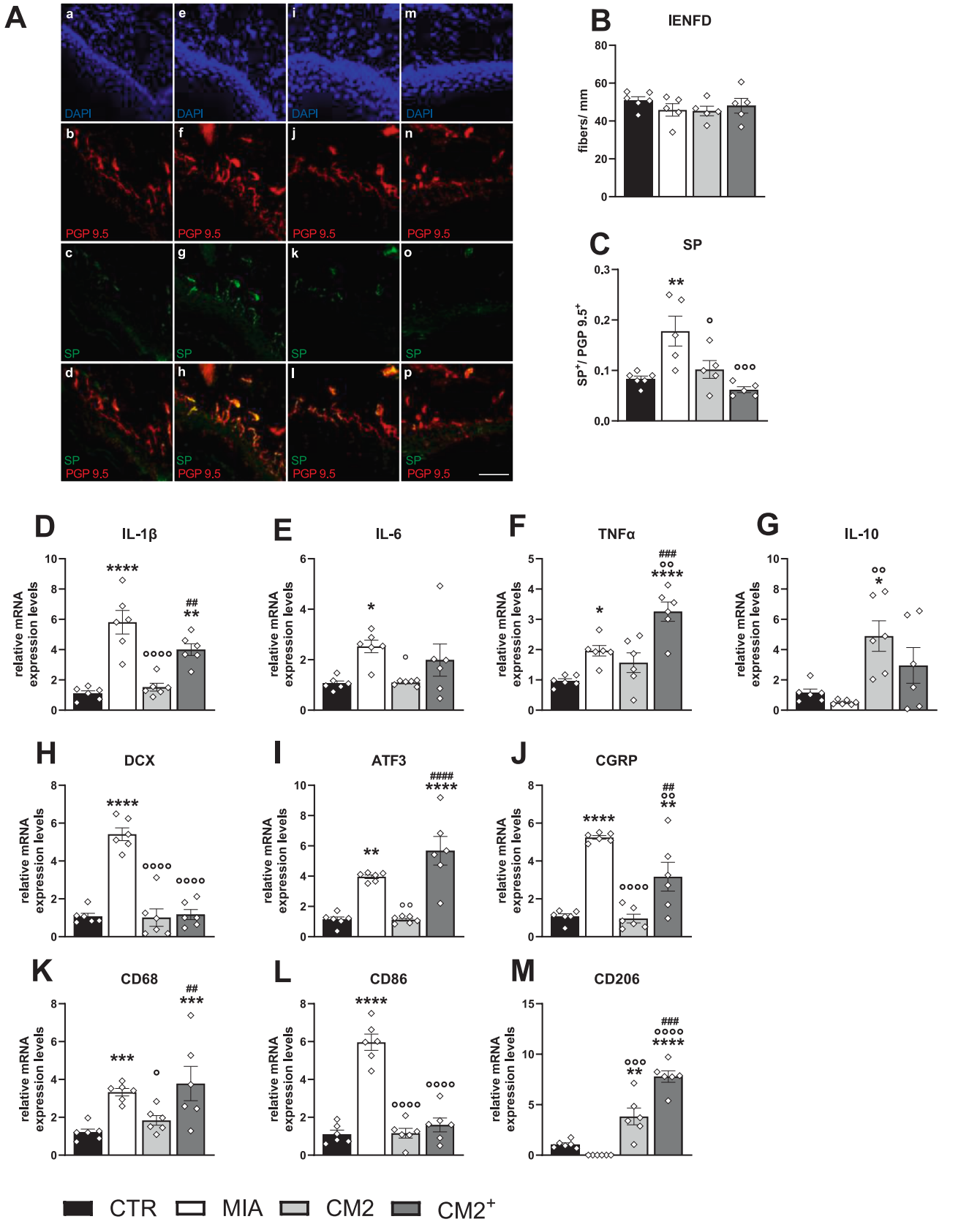

(caption on next page)

Fig. 4. Skin paw and knee biochemical evaluations. Tissues were collected at the end of the experimental protocol (24 days post-OA induction, i.e. 17 days after CMs-treatment). (**A**) Representative immunofluorescence images of (a-d) CTR, (e-h) MIA, (i-l) CM2- and (m-p) $CM2^{+}$-treated mice; (**B**) quantification of intra-epidermal nerve fiber density-(IENFD); (**C**) expression of Substance P-(SP) as ratio to the total PGP 9.5 positive area in epidermal and subepidermal regions. IENFD mean value was calculated in at least 2 sections per animal; SP and PGP 9.5 immunoreactivity were assessed in at least 6 arbitrary fields per animal. Scale bar = 50 μm. (D-M) Knee mRNA levels of: the pro-inflammatory cytokines (**D**) IL-1β, (**E**) IL-6, (**F**) TNFα, (**G**) and anti-inflammatory cytokine IL-10, (**H**) the neurogenesis marker DCX, (**I**) the cellular damage marker ATF3, (**J**) the neuropeptide CGRP and the macrophage markers CD68 (**K**), the pro-inflammatory macrophage marker CD86 (**L**) and the anti-inflammatory macrophage marker CD206 (**M**) were assessed by RT-qPCR. Data were normalized to GAPDH expression and presented as fold-changes over CTR mice group. All data are expressed as mean ± SEM of 5–6 animals/group. Statistical analysis was performed by One-way ANOVA followed by Tukey post hoc test. *p < 0.05, **p < 0.01, ***p < 0.001, ****p < 0.0001 vs. CTR; °p < 0.05, °°p < 0.01, °°°p < 0.001, °°°°p < 0.0001 vs. MIA; ##p < 0.01, ###p < 0.001, ####p < 0.0001 vs. CM2.

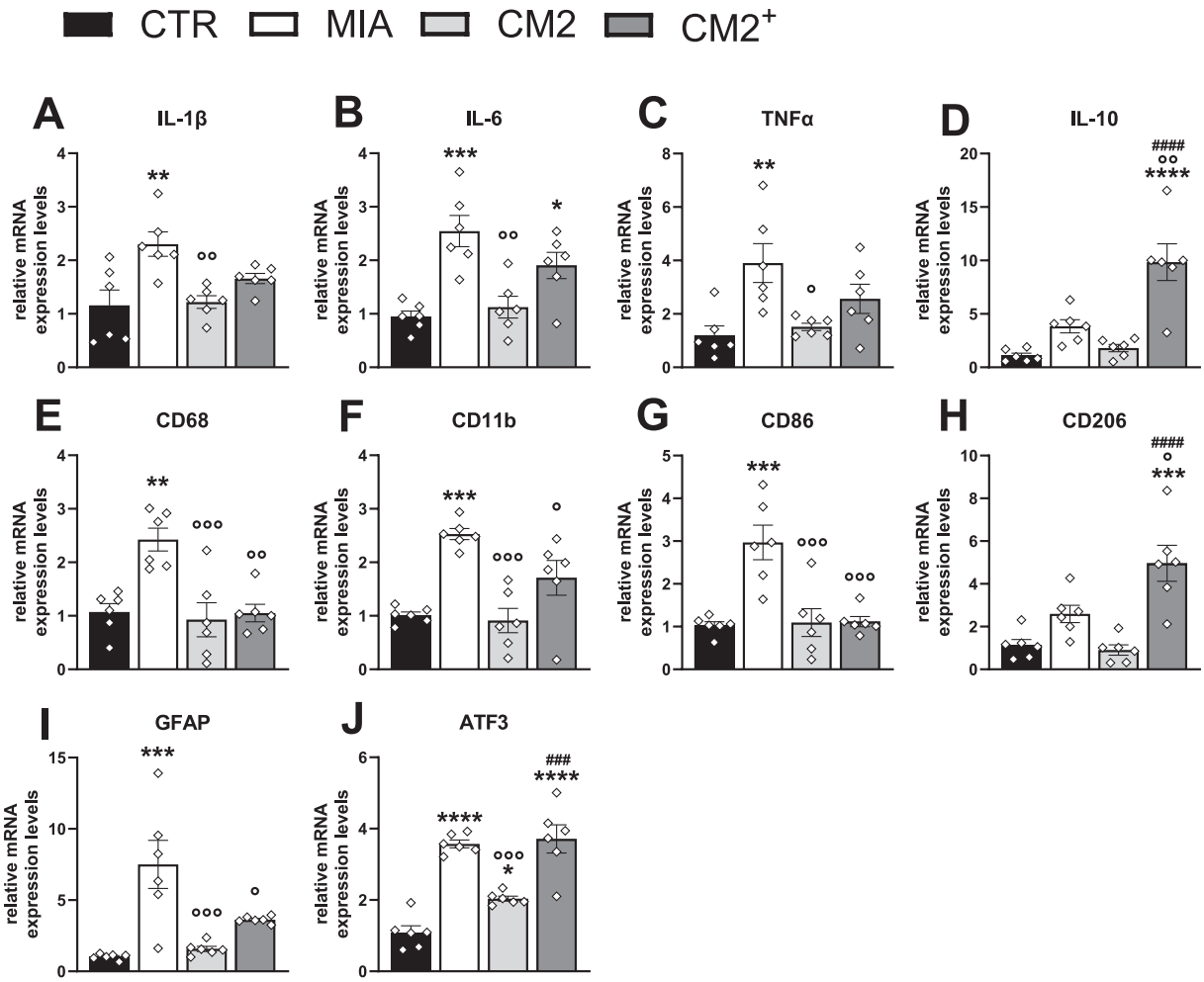

Fig. 5. Sciatic nerve biochemical evaluations. Tissues were collected at the end of the experimental protocol (24 days post-OA induction, i.e. 17 days after CMs-treatment). Levels of the pro-inflammatory cytokines (**A**) IL-1β, (**B**) IL-6 and (**C**) TNFα, (**D**) the anti-inflammatory cytokine IL-10, (**E-F**) the macrophage markers CD68 and CD11b, (**G**) the pro-inflammatory macrophage marker CD86 and (**H**) the anti-inflammatory macrophage marker CD206, (**I**) the Schwann cell marker GFAP, and (**J**) the cellular damage marker ATF3 were assessed by RT-qPCR. Data were normalized to GAPDH expression and presented as fold-changes over CTR mice group. Data are expressed as mean ± SEM of 6 animals/group. Statistical analysis was performed by One-way ANOVA followed by Tukey post hoc test. *p < 0.05, **p < 0.01, ***p < 0.001, ****p < 0.0001 vs. CTR; °p < 0.05, °°p < 0.01, °°°p < 0.001 vs. MIA; ###p < 0.001, ####p < 0.0001 vs. CM2.

and TNFα (Fig. 4D-F) were increased along with a reduction of the anti-inflammatory cytokine IL-10 (Fig. 4G). CM2 showed particularly active in rebalancing the pro-/anti-inflammatory cytokine pattern with respect to $CM2^{+}$. The neurogenesis marker DCX, the cellular damage marker ATF3 and the nociceptive neuronal peptide CGRP were also increased in OA (Fig. 4H-J). Moreover, a general activation of macrophages was observed (CD68, Fig. 4K); a more detailed analysis revealed that this increase is sustained by M1 macrophages (CD86, Fig. 4L) in parallel with a reduced polarization of macrophages toward an M2 phenotype (CD206, Fig. 4M). Also on these parameters, the effect of CM2 was almost always higher than that of $CM2^{+}$. However, it is interesting to note the significant increase in the inflammatory resolving macrophage marker CD206 after both CM2 and $CM2^{+}$ administration.

3.4. *Neuroinflammation in PNS and modulation by CM and CM^{+}*

Overexpression of pro-inflammatory cytokines was observed in the sciatic nerve of MIA-treated animals, and only CM2 significantly restored them to physiological levels (Fig. 5A-C). Moreover, we observed increased levels of all macrophage markers (Fig. 5E-G), GFAP, which is likely to mark Schwann cells (Fig. 5I) and ATF3 (Fig. 5J). Both CM2 and $CM2^{+}$ similarly reduced macrophage and Schwann cell

activation, while only CM2 can prevent the increase in the cellular damage signal ATF3. It is interesting to note that in mice treated with $CM2^{+}$ we found a significant augmentation of the anti-inflammatory cytokine IL-10 and CD206, a marker of type 2 macrophages (Fig. 5D and 5H), while this modulation was not present in CM2-treated animals.

The expression of cytokines (IL-1β, IL-6, TNFα and IL-10) and neuroinflammatory markers (Iba1, CD68, CD11b, CD86, CD206 for macrophage; GFAP for satellite glial cells; ATF3 for cellular damage and CGRP as pronociceptive mediator) in DRG are reported in Fig. 6A-L. All parameters were significantly increased in this tissue, demonstrating the presence of neuroinflammation in MIA mice. A modulation of the neuroinflammation-related markers is exerted by both CM2 and $CM2^{+}$ treatments. However, while treatment with CM2 reduced the overexpression of all cytokines and markers, $CM2^{+}$ restored only some of the altered mRNA levels, such as IL-1β, CD86, CD206, GFAP and ATF3. Moreover, as reported in Fig. 6M, we confirmed by Western blot the

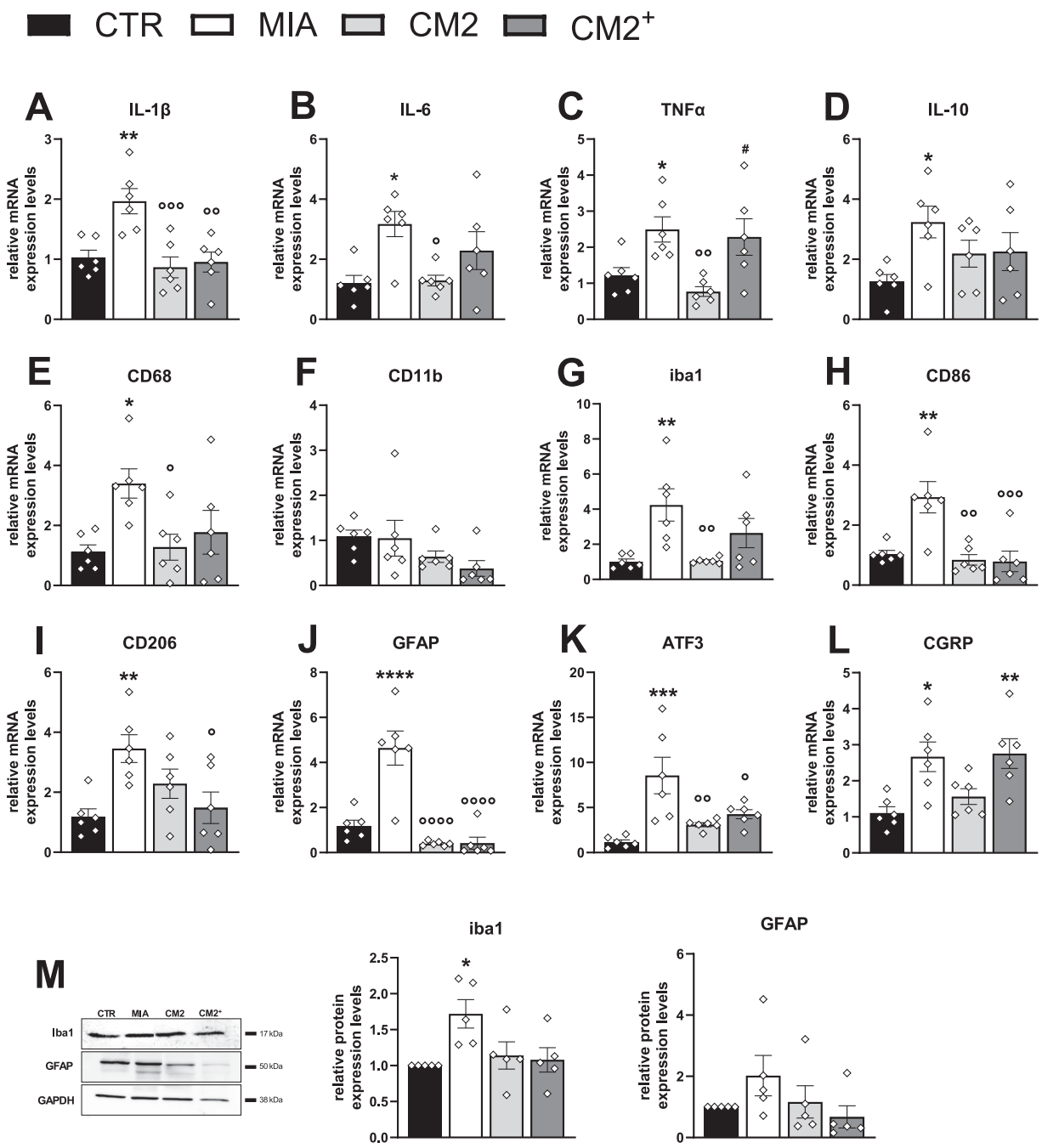

Fig. 6. DRG biochemical evaluations. Tissues were collected at the end of the experimental protocol (24 days post-OA induction, i.e. 17 days after CMs-treatment). Levels of the pro-inflammatory cytokines (**A**) IL-1β, (**B**) IL-6 and (**C**) TNFα, (**D**) the anti-inflammatory cytokine IL-10, (**E-G**) the macrophage markers CD68, CD11b, and Iba1, (**H**) the pro-inflammatory macrophage marker CD86 and (**I**) the anti-inflammatory macrophage marker CD206, (**J**) the satellite glia cell marker GFAP, (**K**) the cellular damage marker ATF3 and (**L**) neuropeptide CGRP were assessed by means of RT-qPCR. Data were normalized to GAPDH expression and presented as fold-changes over CTR mice group. (**M**) Protein levels of Iba1 and GFAP were also evaluated by Western blot analysis. Bands were quantified by densitometry and normalized on GAPDH. Representative bands were reported. Data are expressed as mean ± SEM of 6 (A-L) or 5 (M) animals/group. Statistical analysis was performed by One-way ANOVA followed by Tukey post hoc test. *$p < 0.05$, **$p < 0.01$, ***$p < 0.001$, ****$p < 0.0001$ vs. CTR; °$p < 0.05$, °°$p < 0.01$, °°°$p < 0.001$, °°°°$p < 0.0001$ vs. MIA.

increase as protein-level of macrophage (Iba1) and satellite glial cell activation (GFAP) markers, and how treatments with CM2 and CM2^{+} partially reduced them.

3.5. Neuroinflammation in the central nervous system and its modulation by CM and CM^{+}

Considering that OA mice exhibit altered mood-related behaviors, we checked the cytokine pattern, and the expression of astrocyte (GFAP) and microglia (CD11b, CD86 and CD206) markers in the prefrontal cortex (PFC; Fig. 7A-G) and hippocampus (Fig. 7H-N). In PFC, a significant overexpression of IL-1β and TNFα was present in MIA animals, along with higher levels of the CD86 markers, which can be related to pro-inflammatory activated microglia, while no sign of astrogliosis was observed. Also in this tissue, the treatment with CM2 reduced all the altered parameters, while CM2^{+} affected only TNFα. Similarly, pro-

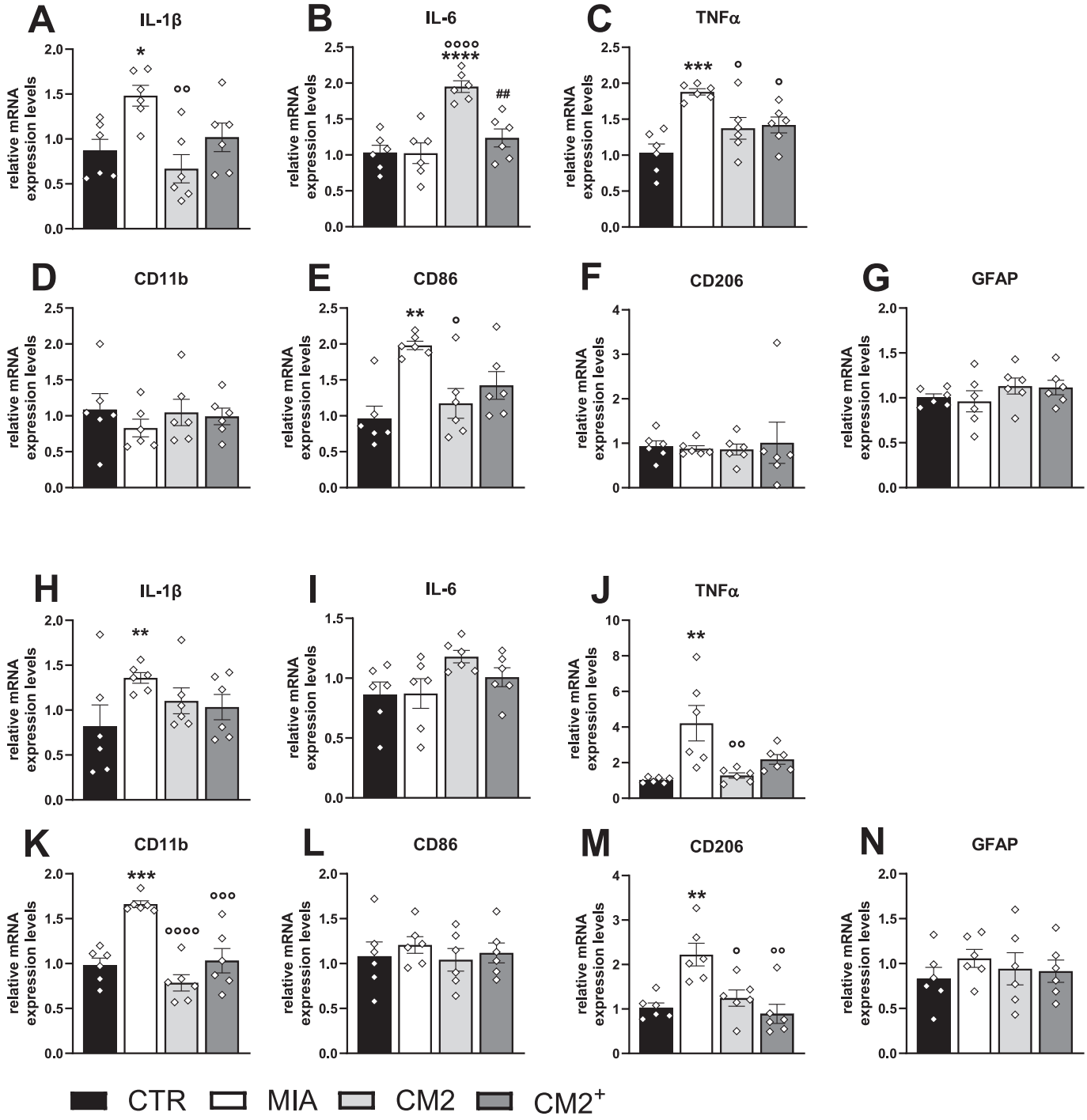

Fig. 7. Brain area biochemical evaluations. Tissues were obtained at the end of the experimental protocol (24 days post-OA induction, i.e. 17 days after CMs-treatment). (**A-G**) Prefrontal cortex and (**H-N**) hippocampus mRNA levels of the pro-inflammatory cytokines (**A,H**) IL-1β, (**B,I**) IL-6 and (**C,J**) TNFα, (**D-F, K-M**) the pro-inflammatory microglial markers CD11b, CD86, and the anti-inflammatory microglia marker CD206 and (**G,N**) astrocytic marker GFAP were assessed by means of RT-qPCR. Data were normalized to GAPDH expression and presented as fold-changes over CTR mice group. Data are expressed as mean ± SEM of 6 animals/group. Statistical analysis was performed by One-way ANOVA followed by Tukey post hoc test. *p < 0.05, **p < 0.01, ***p < 0.001, ****p < 0.0001 vs. CTR; °p < 0.05, °°p < 0.01, °°°p < 0.001, °°°°p < 0.0001 vs. MIA; ##p < 0.01 vs. CM2.

inflammatory cytokines were also elevated in the hippocampus in OA mice, in parallel with the overexpression of the microglia activation markers CD11b and CD206, the latter related to an inflammatory resolving profile. Both treatments with CM2 and CM2$^+$ counteracted the increase of the neuroinflammatory markers, without relevant differences.

4. Discussion

Safe and effective treatment for OA pain remains an unmet medical need. Current analgesic drugs are only minimally effective, their effects are short-lived, and they are often accompanied by adverse effects, especially in the elderly population (Giaretta et al., 2024; Moretti et al., 2024; Pickering et al., 2024). In this study, we confirm that the administration of ASC-CM is an effective and long-lasting approach to pain relief in an OA murine model. Moreover, we demonstrate for the first time that CM also counteracts the development of psychiatric comorbidities often associated with chronic pain.

Additionally, we begin to consider several critical issues that need to be addressed before fully translating this novel treatment to patients, such as the optimal dose, timing of administration, and whether manipulation of stem/stromal cells before collecting media could enhance its efficacy. Indeed, it is widely accepted that when MSCs reach damaged or inflammatory environments they exert their therapeutic effects by secreting soluble factors and EVs, which in turn act in a paracrine manner to modulate the pathological milieu (Alvites et al., 2022). Consequently, inflammatory preconditioning has been proposed as a technique to increase the secretory activity and immunomodulatory properties of MSCs. Although this approach proved promising in some *in vitro* and *in vivo* conditions (Giannasi et al., 2024; Mead et al., 2020; Prasanna et al., 2010; Tolstova et al., 2023; Wang et al., 2024; Waterman et al., 2010), our results indicate that CM obtained from ASCs without pro-inflammatory preconditioning is more effective in controlling both pain and mood alterations in OA mice. It can be speculated that when MSC secretion is induced solely by starvation, i.e. without pro-inflammatory conditioning, the resulting CM is more balanced, containing both pro- and anti-inflammatory mediators and growth factors. Indeed, present results and previous data from us (Giannasi et al., 2024), showing the analysis of CM from preconditioned ASCs, indicate that the enrichment in pro-inflammatory mediators, such as IL-8 and chemokines, greatly exceeds that of anti-inflammatory factors such as IL-4 and IL-10. This finding could be useful for broader clinical applications, as the lack of the preconditioning step in culture highly reduces the variability that might arise from more complex cell culture conditions. However, we acknowledge that we tested only one preconditioning protocol, and that other methods may prove more useful or effective. The antiallodynic and antihyperalgesic effects of both CM and CM$^+$ are dose-dependent. CM derived from two million MSCs (CM2) exerted full analgesic activity, while CM from one million cells (CM1) was less efficacious, though still effective. We also want to highlight that a single injection of CM2 induces rapid and long-lasting pain relief, that starts within a few hours and persists even 17 days after administration. This rapid and sustained analgesic effect of a single ASC-CM injection has been observed in various rodent models of chronic pain, including neuropathic and inflammatory pain (Brini et al., 2017; Guo et al., 2011; L et al., 2019). We are aware that translating the duration of effects from rodent models to humans must be done with caution. In the present study, the term long lasting is used in a preclinical, model-specific context. Based on our experience with pain in the MIA-induced osteoarthritis model (Amodeo et al., 2024), we have consistently observed that other conventional analgesic treatments (e.g., diclofenac or morphine) require chronic daily administration to achieve sustained antihyperalgesic and antiallodynic effects, while the analgesic effects of a single acute administration of these compounds typically dissipate within hours (Amodeo et al., 2022; Galimberti et al., 2023). The prolonged analgesic effect observed after a single administration of ASC-CM, persisting for up to 17 days, represents a clear and meaningful difference within this experimental model (Amodeo et al., 2022; Galimberti et al.,2023). Interestingly, the long-lasting effect of the CM-based approach may be comparable to that exerted by biological drugs such as monoclonal antibodies or soluble receptors.

Persistent pain often correlates with anxiety- and depression-like behaviors. Our results align with recent preclinical studies showing that MIA-treated animals exhibit psychiatric-like features (Amodeo et al., 2023; Amodeo et al., 2025; Amodeo et al., 2024; Batalle et al., 2021; Batalle et al., 2019; Carcole et al., 2019a; Carcole et al., 2019b; Galimberti et al., 2023; La Porta et al., 2015). Notably, a single administration of CM2 and CM2$^+$ effectively prevented the development of both anxiety and depression-like behaviors. There appears to be a good correlation between pain relief and the prevention of psychiatric alterations: only CMs from 2 million cells can reduce both, with CM2 being more effective than CM2$^+$. This underscores the importance of a prompt and effective analgesic treatment to prevent the development of psychiatric comorbidities associated with chronic pain.

The effects of CM are exerted at multiple levels within the organism and across various tissues involved in pain transduction, transmission, and modulation. For example, in our OA model, we did not observe changes in IENFD, indicating that OA-related pain mechanisms are different from pure neuropathic conditions (Brini et al., 2017; Johnson et al., 2008; Lauria et al., 2005). However, the elevated SP levels in the OA-paw skin suggest the presence of neurogenic inflammation. Both CM2 and CM2$^+$ prevent this phenomenon, likely by interrupting the pathological loop induced by SP, which further sensitizes nociceptors (Moussaoui et al., 1993; Seidel et al., 2022). As expected, significant inflammation was present in OA knee joint of MIA animals, characterized by increased pro-inflammatory cytokines, markers of activated M1 macrophages, and decreased IL-10. Treatment with both CMs restored the balance between pro- and anti-inflammatory cytokines and promoted a shift toward M2 macrophage phenotypes. The ability of MSC-derived CMs to activate anti-inflammatory pathways and M2 macrophages is emerging as a key mechanism underlying their therapeutic effects (Bai et al., 2020; Guillen et al., 2018; Heo et al., 2019; Kamada et al., 2021; Liu et al., 2020).

The observation that CM2$^+$ is less effective on TNFα and ATF3, that are not reduced but even increased, may partially explain the less efficacy of the CM2$^+$ on pain. It can also be hypothesized that the increased damage, shown by high level of TNFα and ATF3, induces a reactive stimulation of M2 macrophages that try to counteract it.

Furthermore, CM administration positively impacted alterations in PNS. The sciatic nerve showed signs of neuroinflammation, with activated GFAP-expressing Schwann cells and infiltrating macrophages producing pro-inflammatory cytokines that stimulate nociceptors. Both CM2 and CM2$^+$ reduced the burden of activated cells and inflammatory mediators, although the effects of CM2 were more consistent across all the parameters. Similarly, in the DRG, a critical site for pain processing, CM2 more effectively controlled neuroinflammation, reducing the overexpression of markers for satellite glial cells and macrophages, cytokine levels, and elevated CGRP expression, a key pronociceptive mediator produced by sensory neurons. This indicates that CM not only modulates neuroinflammation but also directly or indirectly influences neuronal activity (Russell et al., 2014). Overall, the extent of the effects of CM2 and CM2$^+$ on behavioral parameters correlates with their impact on neuroinflammation. While both formulations controlled pain, motor deficits, and psychiatric behaviors, CM2 demonstrated a greater efficacy. Both CMs reduced joint and PNS inflammation, but the effects of CM2 were more consistent and pronounced.

Persistent pain can induce changes in brain regions such as the hippocampus and prefrontal cortex, which are crucial for mood regulation (Amodeo et al., 2023; Amodeo et al., 2025; Amodeo et al., 2024; Batalle et al., 2021; Batalle et al., 2019; Carcole et al., 2019a; Carcole et al., 2019b; Galimberti et al., 2023; La Porta et al., 2015; Narita et al., 2006; Suzuki et al., 2007). We observed increased mRNA levels of pro-

inflammatory cytokines IL-1β and TNF-α, along with upregulation of the microglia marker CD86, which is commonly associated with neuroinflammation (Khan et al., 2020; Levy et al., 2018). Interestingly, GFAP expression remained unchanged, suggesting no astrogliosis at this stage. These alterations were also present in the hippocampus, with elevated cytokines and signs of microgliosis. Previous studies from our group suggest that astrocyte involvement may occur at later time points, as GFAP levels increase over time post-OA induction (Amodeo et al., 2025; Galimberti et al., 2023). Importantly, treatment with CMs prevented the onset of neuroinflammatory status in these supraspinal regions, highlighting their potential to mitigate central mechanisms underlying pain-related emotional disturbances.

We acknowledge that the precise sequence of events following systemic CM administration remains to be fully elucidated. It is possible that CMs initially act peripherally, reducing joint inflammation and nociceptor sensitization, decreasing neuroinflammatory signaling from the periphery to CNS. Additionally, given that CMs can cross the nerve-blood and blood–brain barriers (Soares et al., 2022; Yoo et al., 2025), a direct central effect cannot be excluded. Previous work from our group demonstrated that intravenous injection of CM was more effective than its intra-articular administration in OA pain (Amodeo et al., 2021a; Brini et al., 2017), supporting the idea that systemic administration allows CMs to reach multiple sites, including CNS, and to exert their effects more broadly. This multi-level action underscores the potential of CM therapy not only to alleviate pain but also to address mood disturbances associated with chronic OA pain.

As already discussed, CM obtained from stem/stromal cells with only serum starvation is more effective than CM collected after pro-inflammatory conditioning on most of the parameters evaluated. This observation highlights that the quality and quantity of factors in CM are relevant for optimal biological activities. We must underline that in CM both soluble factors and exosomes are present (Niada et al., 2021), and at present we cannot state the relevance of each of them. Certainly, EV carry specific mRNA or miRNA, which could potentiate the reparative and healing process of injured tissues. Although, it is possible that for different pathological conditions, diverse mediators may be responsible for the CM beneficial effect, we think that what makes the secretome unique is the simultaneous presence of all these multiple factors (Peshkova et al., 2023; Soukup et al., 2023; Trigo et al., 2025).

In summary, our findings suggest that MSC-secretome represents a promising, safe, and long-lasting therapeutic approach for OA pain and its psychiatric comorbidities, especially when derived from cells without pro-inflammatory preconditioning. Further research is needed to optimize dosing, timing, and delivery methods, as well as to understand the precise mechanisms involved. Nonetheless, these results pave the way for future clinical translation, offering hope for more effective management of osteoarthritis pain and related comorbidities.

CRediT authorship contribution statement

Giada Amodeo: Writing – original draft, Visualization, Validation, Project administration, Methodology, Investigation, Formal analysis, Data curation, Conceptualization. **Stefania Niada:** Writing – original draft, Visualization, Validation, Project administration, Methodology, Investigation, Funding acquisition, Formal analysis, Data curation, Conceptualization. **Giulia Galimberti:** Writing – review & editing, Visualization, Validation, Investigation. **Silvia Franchi:** Writing – review & editing, Visualization, Validation, Investigation. **Elena Della Morte:** Writing – review & editing, Visualization, Validation, Investigation. **Michela Taiana:** Writing – review & editing, Visualization, Validation, Investigation. **Simona Piccolo:** Writing – review & editing, Visualization, Validation, Investigation. **Stefania Ceruti:** Writing – review & editing, Visualization, Validation. **Laura de Girolamo:** Writing – review & editing, Visualization, Validation. **Anna Teresa Brini:** Writing – original draft, Supervision, Funding acquisition, Conceptualization. **Paola Sacerdote:** Writing – original draft, Supervision, Funding acquisition, Conceptualization.

Funding

The research was supported and funded by the Italian Ministry of Health – "Ricerca Corrente" and by the Department of Biomedical, Surgical, and Dental Sciences of the University of Milan – PSR2023_DIP_017. Galimberti G. is supported by the XXXVIII cycle of the Doctorate in Pharmacological Biomolecular Sciences, Experimental and Clinical, Università degli Studi di Milano, Milan, Italy. Riboldi B. is supported by the XXXIX cycle of the Doctorate in Intersectoral Innovation, Università degli Studi di Milano, Milan, Italy.

Declaration of competing interest

The authors declare that they have no known competing financial interests or personal relationships that could have appeared to influence the work reported in this paper.

Appendix A. Supplementary data

Supplementary data to this article can be found online at https://doi.org/10.1016/j.bbi.2026.106297.

Data availability

Data supporting the findings of this study are publicly available in the Zenodo repository at https://zenodo.org/records/18311059.

References

Alvites, R., Branquinho, M., Sousa, A.C., Lopes, B., Sousa, P., Mauricio, A.C., 2022. Mesenchymal Stem/Stromal Cells and their Paracrine Activity-Immunomodulation Mechanisms and how to Influence the Therapeutic potential. Pharmaceutics 14.

Amodeo, G., Franchi, S., D'Agnelli, S., Galimberti, G., Baciarello, M., Bignami, E.G., Sacerdote, P., 2023. Supraspinal neuroinflammation and anxio-depressive-like behaviors in young- and older- adult mice with osteoarthritis pain: the effect of morphine. Psychopharmacology 240, 2131–2146.

Amodeo, G., Franchi, S., Galimberti, G., Comi, L., D'Agnelli, S., Baciarello, M., Bignami, E.G., Sacerdote, P., 2022. Osteoarthritis Pain in Old mice Aggravates Neuroinflammation and Frailty: the positive effect of Morphine Treatment. Biomedicines 10.

Amodeo, G., Galimberti, G., Ceruti, S., Riboldi, B., Franchi, S., Sacerdote, P., 2025. Physical exercise ameliorates pain, mood alterations and neuroinflammation in a murine model of osteoarthritis. Life Sci. 374, 123710.

Amodeo, G., Magni, G., Galimberti, G., Riboldi, B., Franchi, S., Sacerdote, P., Ceruti, S., 2024. Neuroinflammation in osteoarthritis: from pain to mood disorders. Biochem. Pharmacol. 228, 116182.

Amodeo, G., Niada, S., Moschetti, G., Franchi, S., Savadori, P., Brini, A.T., Sacerdote, P., 2021a. Secretome of human adipose-derived mesenchymal stem cell relieves pain and neuroinflammation independently of the route of administration in experimental osteoarthritis. Brain Behav. Immun. 94, 29–40.

Amodeo, G., Verduci, B., Sartori, P., Procacci, P., Conte, V., Balboni, G., Sacerdote, P., Franchi, S., 2021b. The Antagonism of the Prokineticin System Counteracts Bortezomib Induced Side Effects: Focus on Mood Alterations. Int. J. Mol. Sci. 22.

Axford, J., Butt, A., Heron, C., Hammond, J., Morgan, J., Alavi, A., Bolton, J., Bland, M., 2010. Prevalence of anxiety and depression in osteoarthritis: use of the Hospital anxiety and Depression Scale as a screening tool. Clin. Rheumatol. 29, 1277–1283.

Bai, X., Li, J., Li, L., Liu, M., Liu, Y., Cao, M., Tao, K., Xie, S., Hu, D., 2020. Extracellular Vesicles from Adipose Tissue-Derived Stem Cells Affect notch-miR148a-3p Axis to Regulate Polarization of Macrophages and Alleviate Sepsis in mice. Front. Immunol. 11, 1391.

Barcelon, E.E., Cho, W.H., Jun, S.B., Lee, S.J., 2019. Brain Microglial Activation in Chronic Pain-Associated Affective Disorder. Front. Neurosci. 13, 213.

Barrachina, L., Remacha, A.R., Romero, A., Vitoria, A., Albareda, J., Prades, M., Roca, M., Zaragoza, P., Vazquez, F.J., Rodellar, C., 2018. Assessment of effectiveness and safety of repeat administration of proinflammatory primed allogeneic mesenchymal stem cells in an equine model of chemically induced osteoarthritis. BMC Vet. Res. 14, 241.

Batalle, G., Bai, X., Pouso-Vazquez, E., Roch, G., Rodriguez, L., Pol, O., 2021. The Recovery of Cognitive and Affective Deficiencies Linked with Chronic Osteoarthritis Pain and Implicated Pathways by Slow-Releasing Hydrogen Sulfide Treatment. Antioxidants (Basel) 10.

Batalle, G., Cabarga, L., Pol, O., 2019. The Inhibitory Effects of Slow-Releasing Hydrogen Sulfide Donors in the Mechanical Allodynia, Grip Strength Deficits, and Depressive-Like Behaviors Associated with Chronic Osteoarthritis Pain. Antioxidants (Basel) 9.

Brini, A.T., Amodeo, G., Ferreira, L.M., Milani, A., Niada, S., Moschetti, G., Franchi, S., Borsani, E., Rodella, L.F., Panerai, A.E., Sacerdote, P., 2017. Therapeutic effect of human adipose-derived stem cells and their secretome in experimental diabetic pain. Sci. Rep. 7, 9904.
Carcole, M., Kummer, S., Goncalves, L., Zamanillo, D., Merlos, M., Dickenson, A.H., Fernandez-Pastor, B., Cabanero, D., Maldonado, R., 2019a. Sigma-1 receptor modulates neuroinflammation associated with mechanical hypersensitivity and opioid tolerance in a mouse model of osteoarthritis pain. Br. J. Pharmacol. 176, 3939–3955.
Carcole, M., Zamanillo, D., Merlos, M., Fernandez-Pastor, B., Cabanero, D., Maldonado, R., 2019b. Blockade of the Sigma-1 Receptor Relieves Cognitive and Emotional Impairments Associated to Chronic Osteoarthritis Pain. Front. Pharmacol. 10, 468.
El-Tallawy, S.N., Nalamasu, R., Salem, G.I., LeQuang, J.A.K., Pergolizzi, J.V., Christo, P. J., 2021. Management of Musculoskeletal Pain: an Update with Emphasis on Chronic Musculoskeletal Pain. Pain Ther. 10, 181–209.
Facer, P., Casula, M.A., Smith, G.D., Benham, C.D., Chessell, I.P., Bountra, C., Sinisi, M., Birch, R., Anand, P., 2007. Differential expression of the capsaicin receptor TRPV1 and related novel receptors TRPV3, TRPV4 and TRPM8 in normal human tissues and changes in traumatic and diabetic neuropathy. BMC Neurol. 7, 11.
Galimberti, G., Amodeo, G., Magni, G., Riboldi, B., Balboni, G., Onnis, V., Ceruti, S., Sacerdote, P., Franchi, S., 2023. Prokineticin System is a Pharmacological Target to Counteract Pain and its Comorbid Mood Alterations in an Osteoarthritis Murine Model. Cells 12.
Geraghty, T., Winter, D.R., Miller, R.J., Miller, R.E., Malfait, A.M., 2021. Neuroimmune interactions and osteoarthritis pain: focus on macrophages. Pain Rep 6, e892.
Giannasi, C., Della Morte, E., Cadelano, F., Valenza, A., Casati, S., Dei Cas, M., Niada, S., Brini, A.T., 2024. Boosting the therapeutic potential of cell secretome against osteoarthritis: Comparison of cytokine-based priming strategies. Biomed. Pharmacother. 170, 115970.
Giannasi, C., Niada, S., Magagnotti, C., Ragni, E., Andolfo, A., Brini, A.T., 2020. Comparison of two ASC-derived therapeutics in an in vitro OA model: secretome versus extracellular vesicles. Stem Cell Res Ther 11, 521.
Giaretta, S., Magni, A., Migliore, A., Natoli, S., Puntillo, F., Ronconi, G., Santoiemma, L., Sconza, C., Viapiana, O., Zanoli, G., 2024. A Review of Current Approaches to Pain Management in Knee Osteoarthritis with a Focus on Italian Clinical Landscape. J. Clin. Med. 13.
Goldenberg, D.L., 2010. The interface of pain and mood disturbances in the rheumatic diseases. Semin. Arthritis Rheum. 40, 15–31.
Guillen, M.I., Platas, J., Perez Del Caz, M.D., Mirabet, V., Alcaraz, M.J., 2018. Paracrine Anti-inflammatory Effects of Adipose Tissue-Derived Mesenchymal Stem Cells in Human Monocytes. Front. Physiol. 9, 661.
Guo, W., Wang, H., Zou, S., Gu, M., Watanabe, M., Wei, F., Dubner, R., Huang, G.T., Ren, K., 2011. Bone marrow stromal cells produce long-term pain relief in rat models of persistent pain. Stem Cells 29, 1294–1303.
Heo, J.S., Choi, Y., Kim, H.O., 2019. Adipose-Derived Mesenchymal Stem Cells Promote M2 Macrophage Phenotype through Exosomes. Stem Cells Int. 2019, 7921760.
Jammes, M., Contentin, R., Audigie, F., Casse, F., Galera, P., 2023. Effect of pro-inflammatory cytokine priming and storage temperature of the mesenchymal stromal cell (MSC) secretome on equine articular chondrocytes. Front. Bioeng. Biotechnol. 11, 1204737.
Ji, R.R., Nackley, A., Huh, Y., Terrando, N., Maixner, W., 2018. Neuroinflammation and Central Sensitization in Chronic and Widespread Pain. Anesthesiology 129, 343–366.
Johnson, M.S., Ryals, J.M., Wright, D.E., 2008. Early loss of peptidergic intraepidermal nerve fibers in an STZ-induced mouse model of insensate diabetic neuropathy. Pain 140, 35–47.
Johnson, V.L., Hunter, D.J., 2014. The epidemiology of osteoarthritis. Best Pract. Res. Clin. Rheumatol. 28, 5–15.
Kamada, K., Matsushita, T., Yamashita, T., Matsumoto, T., Iwaguro, H., Sobajima, S., Kuroda, R., 2021. Attenuation of knee Osteoarthritis Progression in mice through Polarization of M2 Macrophages by Intra-Articular Transplantation of Non-Cultured Human Adipose-Derived Regenerative Cells. J. Clin. Med. 10.
Khan, A.R., Geiger, L., Wiborg, O., Czeh, B., 2020. Stress-Induced Morphological, Cellular and Molecular changes in the Brain-Lessons Learned from the Chronic Mild stress Model of Depression. Cells 9.
L, P.K., Kandoi, S., Misra, R., S, V., K, R., Verma, R.S., 2019. The mesenchymal stem cell secretome: A new paradigm towards cell-free therapeutic mode in regenerative medicine. Cytokine Growth Factor Rev 46, 1–9.
La Porta, C., Bura, S.A., Llorente-Onaindia, J., Pastor, A., Navarrete, F., Garcia-Gutierrez, M.S., De la Torre, R., Manzanares, J., Monfort, J., Maldonado, R., 2015. Role of the endocannabinoid system in the emotional manifestations of osteoarthritis pain. Pain 156, 2001–2012.
Lauria, G., Lombardi, R., Borgna, M., Penza, P., Bianchi, R., Savino, C., Canta, A., Nicolini, G., Marmiroli, P., Cavaletti, G., 2005. Intraepidermal nerve fiber density in rat foot pad: neuropathologic-neurophysiologic correlation. J. Peripher. Nerv. Syst. 10, 202–208.
Levy, M.J.F., Boulle, F., Steinbusch, H.W., van den Hove, D.L.A., Kenis, G., Lanfumey, L., 2018. Neurotrophic factors and neuroplasticity pathways in the pathophysiology and treatment of depression. Psychopharmacology 235, 2195–2220.
Liu, H., Zhu, X., Cao, X., Chi, A., Dai, J., Wang, Z., Deng, C., Zhang, M., 2021. IL-1beta-primed mesenchymal stromal cells exert enhanced therapeutic effects to alleviate Chronic Prostatitis/Chronic Pelvic Pain Syndrome through systemic immunity. Stem Cell Res Ther 12, 514.
Liu, J., Qiu, P., Qin, J., Wu, X., Wang, X., Yang, X., Li, B., Zhang, W., Ye, K., Peng, Z., Lu, X., 2020. Allogeneic adipose-derived stem cells promote ischemic muscle repair by inducing M2 macrophage polarization via the HIF-1alpha/IL-10 pathway. Stem Cells 38, 1307–1320.
Matsuda, M., Huh, Y., Ji, R.R., 2019. Roles of inflammation, neurogenic inflammation, and neuroinflammation in pain. J. Anesth. 33, 131–139.
Mead, B., Chamling, X., Zack, D.J., Ahmed, Z., Tomarev, S., 2020. TNFalpha-Mediated Priming of Mesenchymal Stem Cells Enhances their Neuroprotective effect on Retinal Ganglion Cells. Invest. Ophthalmol. Vis. Sci. 61, 6.
Moretti, A., Snichelotto, F., Liguori, S., Paoletta, M., Toro, G., Gimigliano, F., Iolascon, G., 2024. The challenge of pharmacotherapy for musculoskeletal pain: an overview of unmet needs. Ther Adv Musculoskelet Dis 16, 1759720X241253656.
Moriarty, O., Finn, D.P., 2014. Cognition and pain. Curr. Opin. Support. Palliat. Care 8, 130–136.
Moriarty, O., McGuire, B.E., Finn, D.P., 2011. The effect of pain on cognitive function: a review of clinical and preclinical research. Prog. Neurobiol. 93, 385–404.
Moussaoui, S., Carruette, A., Garret, C., 1993. Further evidence that substance P is a mediator of both neurogenic inflammation and pain: two phenomena inhibited either by postsynaptic blockade of NK1 receptors or by presynaptic action of opioid receptor agonists. Regul. Pept. 46, 424–425.
Narita, M., Kuzumaki, N., Narita, M., Kaneko, C., Hareyama, N., Miyatake, M., Shindo, K., Miyoshi, K., Nakajima, M., Nagumo, Y., Sato, F., Wachi, H., Seyama, Y., Suzuki, T., 2006. Chronic pain-induced emotional dysfunction is associated with astrogliosis due to cortical delta-opioid receptor dysfunction. J. Neurochem. 97, 1369–1378.
Niada, S., Giannasi, C., Magagnotti, C., Andolfo, A., Brini, A.T., 2021. Proteomic analysis of extracellular vesicles and conditioned medium from human adipose-derived stem/stromal cells and dermal fibroblasts. J. Proteomics 232, 104069.
Noronha, N.C., Mizukami, A., Caliari-Oliveira, C., Cominal, J.G., Rocha, J.L.M., Covas, D. T., Swiech, K., Malmegrim, K.C.R., 2019. Correction to: Priming approaches to improve the efficacy of mesenchymal stromal cell-based therapies. Stem Cell Res Ther 10, 132.
Peshkova, M., Korneev, A., Suleimanov, S., Vlasova, I.I., Svistunov, A., Kosheleva, N., Timashev, P., 2023. MSCs' conditioned media cytokine and growth factor profiles and their impact on macrophage polarization. Stem Cell Res Ther 14, 142.
Pickering, G., Kotlinska-Lemieszek, A., Krcevski Skvarc, N., O'Mahony, D., Monacelli, F., Knaggs, R., Morel, V., Kocot-Kepska, M., 2024. Pharmacological Pain Treatment in older Persons. Drugs Aging 41, 959–976.
Prasanna, S.J., Gopalakrishnan, D., Shankar, S.R., Vasandan, A.B., 2010. Pro-inflammatory cytokines, IFNgamma and TNFalpha, influence immune properties of human bone marrow and Wharton jelly mesenchymal stem cells differentially. PLoS One 5, e9016.
Ragni, E., Perucca Orfei, C., De Luca, P., Mondadori, C., Vigano, M., Colombini, A., de Girolamo, L., 2020. Inflammatory priming enhances mesenchymal stromal cell secretome potential as a clinical product for regenerative medicine approaches through secreted factors and EV-miRNAs: the example of joint disease. Stem Cell Res Ther 11, 165.
Russell, F.A., King, R., Smillie, S.J., Kodji, X., Brain, S.D., 2014. Calcitonin gene-related peptide: physiology and pathophysiology. Physiol. Rev. 94, 1099–1142.
Sassone, J., Taiana, M., Lombardi, R., Porretta-Serapiglia, C., Freschi, M., Bonanno, S., Marcuzzo, S., Caravello, F., Bendotti, C., Lauria, G., 2016. ALS mouse model SOD1G93A displays early pathology of sensory small fibers associated to accumulation of a neurotoxic splice variant of peripherin. Hum. Mol. Genet. 25, 1588–1599.
Seidel, M.F., Hugle, T., Morlion, B., Koltzenburg, M., Chapman, V., MaassenVanDenBrink, A., Lane, N.E., Perrot, S., Zieglgansberger, W., 2022. Neurogenic inflammation as a novel treatment target for chronic pain syndromes. Exp. Neurol. 356, 114108.
Sharma, A., Kudesia, P., Shi, Q., Gandhi, R., 2016. Anxiety and depression in patients with osteoarthritis: impact and management challenges. Open Access Rheumatol. 8, 103–113.
Soares, M.B.P., Goncalves, R.G.J., Vasques, J.F., da Silva-Junior, A.J., Gubert, F., Santos, G.C., de Santana, T.A., Almeida Sampaio, G.L., Silva, D.N., Dominici, M., Mendez-Otero, R., 2022. Current Status of Mesenchymal Stem/Stromal Cells for Treatment of Neurological Diseases. Front. Mol. Neurosci. 15, 883378.
Soukup, R., Gerner, I., Mohr, T., Gueltekin, S., Grillari, J., Jenner, F., 2023. Mesenchymal Stem Cell Conditioned Medium Modulates Inflammation in Tenocytes: complete Conditioned Medium has Superior Therapeutic Efficacy than its Extracellular Vesicle Fraction. Int. J. Mol. Sci. 24.
Suzuki, T., Amata, M., Sakaue, G., Nishimura, S., Inoue, T., Shibata, M., Mashimo, T., 2007. Experimental neuropathy in mice is associated with delayed behavioral changes related to anxiety and depression. Anesth. Analg. 104, 1570–1577 table of contents.
Tolstova, T., Dotsenko, E., Kozhin, P., Novikova, S., Zgoda, V., Rusanov, A., Luzgina, N., 2023. The effect of TLR3 priming conditions on MSC immunosuppressive properties. Stem Cell Res Ther 14, 344.
Tong, L., Yu, H., Huang, X., Shen, J., Xiao, G., Chen, L., Wang, H., Xing, L., Chen, D., 2022. Current understanding of osteoarthritis pathogenesis and relevant new approaches. Bone Res. 10, 60.
Trigo, C.M., Rodrigues, J.S., Camoes, S.P., Sola, S., Miranda, J.P., 2025. Mesenchymal stem cell secretome for regenerative medicine: where do we stand? J. Adv. Res. 70, 103–124.
Wang, C., Jiang, C., Yang, Y., Xi, C., Yin, Y., Wu, H., Qian, C., 2024. Therapeutic potential of HUC-MSC-exos primed with IFN-gamma against LPS-induced acute lung injury. Iran. J. Basic Med. Sci. 27, 375–382.

Waterman, R.S., Tomchuck, S.L., Henkle, S.L., Betancourt, A.M., 2010. A new mesenchymal stem cell (MSC) paradigm: polarization into a pro-inflammatory MSC1 or an Immunosuppressive MSC2 phenotype. PLoS One 5, e10088.

Yoo, D., Jung, S.Y., Go, D., Park, J.Y., You, D.G., Jung, W.K., Li, Y., Ding, J., Park, J.H., Um, W., 2025. Functionalized extracellular vesicles of mesenchymal stem cells for regenerative medicine. J Nanobiotechnology 23, 219.

Zhuo, M., 2016. Neural Mechanisms underlying Anxiety-Chronic Pain Interactions. Trends Neurosci. 39, 136–145.